

# States interpolating between number and coherent states and their interaction with atomic systems

Hongchen Fu\*, Yinqi Feng<sup>†</sup> and Allan I. Solomon<sup>‡</sup>

*Quantum Processes Group, The Open University,  
Milton Keynes, MK7 6AA, UK*

## Abstract

Using the eigenvalue definition of binomial states we construct new intermediate number-coherent states which reduce to number and coherent states in two different limits. We reveal the connection of these intermediate states with photon-added coherent states and investigate their non-classical properties and quasi-probability distributions in detail. It is of interest to note that these new states, which interpolate between coherent states and number states, neither of which exhibit squeezing, are nevertheless squeezed states. A scheme to produce these states is proposed. We also study the interaction of these states with atomic systems in the framework of the two-photon Jaynes-Cummings model, and describe the response of the atomic system as it varies between the pure Rabi oscillation and the collapse-revival mode and investigate field observables such as photon number distribution, entropy and the Q-function.

J.Phys.A:Math.Gen.33 (2000) in press.

---

\*On leave of absence from Institute of Theoretical Physics, Northeast Normal University, Changchun 130024, P. R. China. Email:h.fu@open.ac.uk

<sup>†</sup>Email: y.feng@open.ac.uk

<sup>‡</sup>Email: a.i.solomon@open.ac.uk

# 1 Introduction

Since Stoler, Saleh and Teich proposed the binomial states (BS) in 1985 [1], so-called *intermediate* states which interpolate between some fundamental states such as number states, coherent and squeezed states and phase states have attracted much attention [2].

The BS are finite linear combinations of number states

$$|\eta, M\rangle = \sum_{n=0}^M \left[ \binom{M}{n} \eta^n (1-\eta)^{M-n} \right]^{1/2} |n\rangle, \quad (1.1)$$

where  $M$  is a non-negative integer,  $\eta$  is a *real* probability ( $0 < \eta < 1$ ) and  $|n\rangle$  is a number state of the radiation field. The photon number distribution is clearly a binomial distribution, whence the name *binomial state*. The BS are intermediate number-coherent states in the sense that they reduce to number and coherent states in different limits

$$|\eta, M\rangle \longrightarrow \begin{cases} |M\rangle, & \eta \rightarrow 1, \\ |0\rangle, & \eta \rightarrow 0, \\ |\alpha\rangle, & \eta \rightarrow 0, M \rightarrow \infty, \eta M = \alpha^2. \end{cases} \quad (1.2)$$

The BS also admit an eigenvalue definition [3]

$$\left( \sqrt{\eta}N + \sqrt{1-\eta}\sqrt{M-N}a \right) |\eta, M\rangle = \sqrt{\eta}M |\eta, M\rangle, \quad (1.3)$$

where  $a$ ,  $a^\dagger$  and  $N$  are the annihilation, creation and the number operators, respectively. The algebra involved is the  $\text{su}(2)$  algebra (Holstein-Primakoff realization [4])

$$J^+ = \sqrt{M-N}a, \quad J^- = a^\dagger\sqrt{M-N}, \quad J^3 = \frac{M}{2} - N, \quad (1.4)$$

and in the present case the coherent state limit is essentially the contraction of  $\text{su}(2)$  to the Heisenberg-Weyl algebra generated by  $a^\dagger$ ,  $a$  and 1.

Since number and coherent states are eigenstates of the number operator  $N$  and the annihilation operator  $a$ , respectively, it would seem more natural that, to define states interpolating between number and coherent states, we consider the eigenvalue equation of a linear combination of  $N$  and  $a$  itself (not  $J^+$ ), namely,

$$\left( \sqrt{\eta}N + \sqrt{1-\eta}a \right) \|\eta, \beta\rangle = \beta \|\eta, \beta\rangle. \quad (1.5)$$

Here  $0 < \eta < 1$  as before and  $\beta$  is an eigenvalue which will be determined not only from the eigenvalue equation Eq.(1.5) but also by a *physical requirement* (see Sec. 2).

In this paper we study the states  $\|\eta, \beta\rangle$  and their various properties. We find that for  $\beta = \sqrt{\eta}M$  ( $M$  a non-negative integer), the solutions to Eq. (1.5) are indeed intermediate

states which interpolate between number and coherent states. We also find that these states are closely related to the photon-added coherent states proposed by Agarwal and Tara [5]. The properties of this new state, such as their sub-Poissonian statistics, antibunching effects and squeezing effects, as well as their quasi-probability distributions (the Q and Wigner functions), are studied in detail. Although coherent and number states are not squeezed, the new interpolating states are squeezed, and exhibit highly nonclassical behavior. We also propose a scheme to produce these intermediate states in a cavity.

The intermediate number-coherent states are of particular interest in their interaction with atomic systems. In the context of the Jaynes-Cummings (JC) model, atomic population inversion exhibits two completely different phenomena: Rabi oscillation when the field is initially prepared in a number state; and periodic collapse and revival when the field is initially prepared in a coherent state. We naturally expect that the states proposed in this paper will present phenomena intermediate between Rabi oscillation and periodic collapse-revival, given that the initial state of the field is in an intermediate state. In Sec.6 we study the interaction of the states with the atomic systems based on the two-photon JC model and we indeed observe this intermediate behavior. We also give an analytic derivation of the approximate photon number distribution of the field and find it exhibits strong oscillation at  $\tau = \pi/4, 3\pi/4$  ( $\tau$  the scaled time). This phenomena is explained physically in terms of the entropy and Q-function of the field.

## 2 New intermediate number-coherent states

In this section we solve the eigenvalue equation Eq.(1.5), discuss the relation of the states (1.5) to photon-added coherent states and study the limit to number and coherent states.

### 2.1 Solutions

Expanding the state  $||\eta, \beta\rangle$  in number states

$$||\eta, \beta\rangle = \sum_{n=0}^{\infty} C_n |n\rangle \quad (2.1)$$

inserting it into Eq. (1.5) and comparing the two sides of the equation, we find the solution of the eigenvalue equation Eq.(1.5)

$$||\eta, \beta\rangle = C_0 \sum_{n=0}^{\infty} \frac{[\beta - \sqrt{\eta}(n-1)][\beta - \sqrt{\eta}(n-2)] \cdots \beta}{(\sqrt{1-\eta})^n \sqrt{n!}} |n\rangle, \quad (2.2)$$

where  $C_0$  is the normalization constant. Here, the eigenvalue  $\beta$  is an arbitrary complex number.

It is easy to see that for any complex number  $\beta$  the state Eq.(2.2) reduces to the coherent state  $|\beta\rangle \equiv e^{-\frac{|\beta|^2}{2}} \sum_{n=0}^{\infty} \frac{\beta^n}{\sqrt{n!}} |n\rangle$  in the limit  $\eta \rightarrow 0$ , as expected. However, it does not have a number state limit for arbitrary  $\beta$  since number states are eigenstates of  $N$  with non-negative integer eigenvalues. Further, we would like to have truncated states which are *finite* superpositions of the number states just as the binomial states are. With this in mind, we must choose  $\beta = \sqrt{\eta}M$ , where  $M$  is a non-negative integer. In this case it is easy to see that the coefficients  $C_n$  are truncated

$$C_n = \begin{cases} 0, & \text{when } n > M, \\ \left(\sqrt{\frac{\eta}{1-\eta}}\right)^n \frac{M!}{(M-n)!\sqrt{n!}} C_0, & \text{when } n \leq M. \end{cases} \quad (2.3)$$

Here the normalization constant  $C_0(\eta, M)$  is obtained as

$$C_0(\eta, M) = \left[ \sum_{n=0}^M \left(\frac{\eta}{1-\eta}\right)^n \frac{(M!)^2}{[(M-n)!]^2 n!} \right]^{-\frac{1}{2}} = \frac{\lambda^M}{\sqrt{M! L_M(-\lambda^2)}}, \quad (2.4)$$

where  $\lambda \equiv \sqrt{(1-\eta)/\eta}$  and  $L_M(x)$  is the Laguerre polynomial [6]

$$L_M(x) = \sum_{n=0}^M \frac{1}{n!} \binom{M}{M-n} (-1)^n x^n. \quad (2.5)$$

Inserting Eq. (2.3) and Eq. (2.4) into Eq. (2.1), we obtain the desired solution  $\|\eta, (\beta = \sqrt{\eta}M)\rangle \equiv \|\eta, M\rangle$

$$\|\eta, M\rangle = \frac{1}{\sqrt{M! L_M(-\lambda^2)}} \sum_{n=0}^M \lambda^{M-n} \frac{M!}{(M-n)!\sqrt{n!}} |n\rangle, \quad (2.6)$$

which is a *finite* linear superposition of number states.

We now consider the limiting cases of above state Eq.(2.6) as number and coherent states. First consider the limit  $\eta \rightarrow 1$ . From the number-state expansion Eq.(2.6), it follows that

$$C_n = \frac{\lambda^{M-n} M!}{\sqrt{M! n! (M-n)!}} \longrightarrow \delta_{M,n}, \quad (2.7)$$

namely,  $\|\eta, M\rangle \rightarrow |M\rangle$ . Then, in the different limit  $\eta \rightarrow 0$ ,  $M \rightarrow \infty$  with  $\sqrt{\eta}M = \alpha$  a real constant, we have

$$\frac{M!}{(M-n)!} \rightarrow M^n, \quad \lambda^{-n} M^n \rightarrow \alpha^n, \quad C_0 \rightarrow \exp(-\alpha^2/2). \quad (2.8)$$

and therefore Eq.(2.6) reduces to the coherent state  $|\alpha\rangle$ .

The above discussion shows that the state  $\|\eta, M\rangle$  may be considered as an intermediate state which interpolates between a number state and a coherent state.

## 2.2 Connection with photon-added coherent states

The state Eq.(2.6) can be written in more elegant form. By making use of  $|n\rangle = \frac{a^{\dagger n}}{\sqrt{n!}}|0\rangle$ , we can write Eq.(2.6) as

$$\|\eta, M\rangle = \frac{1}{\sqrt{M!L_M(-\lambda^2)}} \left[ \sum_{n=0}^M \binom{M}{n} (a^\dagger)^n \lambda^{M-n} \right] |0\rangle = \frac{1}{\sqrt{M!L_M(-\lambda^2)}} (a^\dagger + \lambda)^M |0\rangle, \quad (2.9)$$

where we have used the binomial formula.

Furthermore, thanks to the equation (real  $\lambda$  in our case)

$$D(-\lambda)a^\dagger D(\lambda) = a^\dagger + \lambda, \quad (2.10)$$

where  $D(\lambda)$  is the displacement operator

$$D(\lambda) = \exp[\lambda(a^\dagger - a)], \quad (2.11)$$

we can rewrite Eq. (2.9) in the form

$$\begin{aligned} \|\eta, M\rangle &= \frac{1}{\sqrt{M!L_M(-\lambda^2)}} D(-\lambda)a^{\dagger M} D(\lambda)|0\rangle \\ &= \frac{1}{\sqrt{M!L_M(-\lambda^2)}} D(-\lambda)a^{\dagger M} |\lambda\rangle \\ &\equiv D(-\lambda)|\lambda, M\rangle \end{aligned} \quad (2.12)$$

where  $|\lambda\rangle = D(\lambda)|0\rangle$  is a coherent state and

$$|\lambda, M\rangle \equiv \frac{1}{\sqrt{M!L_M(-\lambda^2)}} a^{\dagger M} |\lambda\rangle \quad (2.13)$$

is a so-called *photon-added coherent state* or *excited coherent state* [5]. So from Eq. (2.13) we conclude that our new intermediate number-coherent states are *displaced excited coherent states*.

However, we would like to point out that our states are very different from the photon-added coherent states. The photon-added states are an *infinite* superposition of number states from  $M$  to infinity, while our states are a *finite* superposition of number states from 0 to  $M$ .

## 3 Nonclassical Properties

In this section we shall investigate the statistical and squeezing properties of  $\|\eta, M\rangle$ , with special emphasis on the comparison with those of the BS.

### 3.1 Photon statistics

The easily-derived relation

$$a^k \|\eta, M\rangle = \left[ \frac{M(M-1)\cdots(M-k+1)L_{M-k}(-\lambda^2)}{L_M(-\lambda^2)} \right]^{1/2} \|\eta, M-k\rangle, \quad (3.1)$$

for  $k \leq M$  and  $a^k \|\eta, M\rangle = 0$  for  $k > M$ , gives the mean value of  $\langle N \rangle$  and  $\langle N^2 \rangle$

$$\langle N \rangle = \frac{ML_{M-1}(-\lambda^2)}{L_M(-\lambda^2)}, \quad (3.2)$$

$$\langle N^2 \rangle = \frac{M(M-1)L_{M-2}(-\lambda^2) + ML_{M-1}(-\lambda^2)}{L_M(-\lambda^2)}, \quad (3.3)$$

and Mandel Q-parameter [7]

$$Q(\eta, M) = \frac{\langle N^2 \rangle - \langle N \rangle^2}{\langle N \rangle} - 1 = (M-1) \frac{L_{M-2}(-\lambda^2)}{L_{M-1}(-\lambda^2)} - M \frac{L_{M-1}(-\lambda^2)}{L_M(-\lambda^2)}. \quad (3.4)$$

If  $Q(\eta, M) < 0$  (*resp.*  $Q(\eta, M) > 0$ ), the field in the state  $\|\eta, M\rangle$  is sub-Poissonian (*resp.* super-Poissonian).  $Q(\eta, M) = 0$  corresponds to Poissonian statistics.

For a fixed  $M$ , there are two extreme cases,  $\eta = 0$  (or  $\lambda = \infty$ ) and  $\eta = 1$  (or  $\lambda = 0$ ). It is easy to see that

$$Q(\eta, M) \longrightarrow \begin{cases} -1 & \lambda = 0, \\ 0 & \lambda \rightarrow \infty, \end{cases} \quad (3.5)$$

in agreement with the Q-parameter values for number states and the vacuum state. Here we have used the fact  $L_M(0) = 1$  and  $L_m(x)/L_n(x) \rightarrow 0$  for  $m < n$  and  $x \rightarrow \infty$ .

Fig. 1 is a plot of  $Q(\eta, M)$  with respect to  $\eta$  for  $M = 2, 50, 100$ . The Q-parameter of the binomial states (BS) is also presented in the figure ( $Q = -\eta$  for any  $M$ ). From the figure we observe that the field in  $\|\eta, M\rangle$  is *sub-Poissonian* except for the case  $\eta = 0$ .

We say that a field is antibunched if the second-order correlation function  $g^{(2)}(0) = \langle a^\dagger a^\dagger a a \rangle / \langle a^\dagger a \rangle^2 < 1$  [8]. In fact, the occurrence of antibunching effects and sub-Poissonian statistics coincides for single mode, time-independent fields such as the state  $\|\eta, M\rangle$  of this paper. So the field  $\|\eta, M\rangle$  is antibunched except at the point  $\eta = 0$ .

### 3.2 Squeezing properties

Define two quadratures  $x$  (coordinate) and  $p$  (momentum)

$$x = \frac{1}{\sqrt{2}} (a + a^\dagger), \quad p = \frac{1}{\sqrt{2}i} (a - a^\dagger). \quad (3.6)$$

Then we can easily obtain their variances  $(\Delta x)^2 \equiv \langle x^2 \rangle - \langle x \rangle^2$  and  $(\Delta p)^2 \equiv \langle p^2 \rangle - \langle p \rangle^2$

$$(\Delta x)^2 = \frac{1}{2} + \frac{ML_{M-1}(-\lambda^2)}{L_M(-\lambda^2)} + \frac{\lambda^2 L_{M-2}^{(2)}(-\lambda^2)}{L_M(-\lambda^2)} - 2 \left[ \frac{\lambda L_{M-1}^{(1)}(-\lambda^2)}{L_M(-\lambda^2)} \right]^2, \quad (3.7)$$

$$(\Delta p)^2 = \frac{1}{2} + \frac{ML_{M-1}(-\lambda^2)}{L_M(-\lambda^2)} - \frac{\lambda^2 L_{M-2}^{(2)}(-\lambda^2)}{L_M(-\lambda^2)}, \quad (3.8)$$

where  $L_m^{(k)}(x)$  is the associated Laguerre polynomial defined by [6]

$$L_m^{(k)}(x) = \sum_{n=0}^m \frac{(m+k)!}{(m-n)!n!(k+n)!} (-x)^n, \quad (k > -1). \quad (3.9)$$

If  $(\Delta x)^2 < 1/2$  (or  $(\Delta p)^2 < 1/2$ ), we say the state is *squeezed* in the quadrature  $x$  (or  $p$ ).

Fig.2 is a plot showing how the variance  $(\Delta x)^2$  depends on the parameters  $\eta$  and  $M$ . When  $\eta = 0$ ,  $(\Delta x)^2 = 1/2$  since the state is just the vacuum state and in this case the field is not squeezed. Then, as  $\eta$  increases the field becomes squeezed until maximum squeezing is reached; then the squeezing decreases until it disappears at a point  $\eta_0$  depending on  $M$ . We note that  $\eta_0 < 1$  when  $M > 0$  since  $(\Delta x^2) = M + 1/2 > 1/2$  when  $\eta \rightarrow 1$ .

We also observe from Fig.2 that the larger  $M$ , the stronger the squeezing, and the wider the squeezing range.

It is known that the optimal signal-to-quantum noise ratio for an arbitrary quantum state

$$\rho = \frac{\langle x \rangle^2}{(\Delta x)^2} \quad (3.10)$$

has the value  $4N_s(N_s + 1)$  which is attainable for the usual coherent squeezed state[9]. For a coherent state the maximal ratio is  $4N_s$ , where  $N_s$  is the mean value of the number operator  $N$  for the quantum state.

For the intermediate number-coherent state  $||\eta, M\rangle$ , the signal-to-quantum noise ratios for different parameters  $\eta$  and  $M$  are shown in Fig. 3. The ratio for  $\eta = 0$  and  $\eta = 1$ , which correspond to the vacuum state and number state respectively, is zero. For other  $\eta$ , we find from Fig. 3 (a) that the larger  $M$ , the larger the ratio. Fig.3 (b) gives plots of  $4\langle N \rangle(\langle N \rangle + 1)$  ( $\langle N \rangle$  is given by Eq.(3.2)),  $4\langle N \rangle$  and the ratio for the state  $||\eta, M\rangle$  with  $M = 10$ . We find that

(1) the ratio for  $||\eta, M\rangle$  is always smaller than the value  $4\langle N \rangle(\langle N \rangle + 1)$ , which is in accord with the general result[9];

(2) for some values of  $\eta$  the ratio is larger than  $4\langle N \rangle$ . We observe that the states with ratio larger than  $4\langle N \rangle$  correspond to squeezed states (see Fig. 2.).

## 4 Quasi-probability distributions

Quasi-probability distributions [10] in the coherent state basis turn out to be useful measures for studying the nonclassical features of radiation fields. In this section we study the Q-function (also called the Husimi function) and the Wigner function of the state  $||\eta, M\rangle$ .

One can prove that (see Appendix A), if two states  $|\psi\rangle_\alpha$  and  $|\psi\rangle$  satisfy  $|\psi\rangle_\alpha = D(\alpha)|\psi\rangle$ , where  $D(\alpha) = e^{\alpha a^\dagger - \alpha^* a}$  is the displacement operator, the Q and Wigner functions of  $|\psi\rangle_\alpha$  are simply a displacement of those of  $|\psi\rangle$ , namely

$$Q(\beta)_{|\psi\rangle_\alpha} = Q(\beta - \alpha)_{|\psi\rangle}, \quad W(\beta)_{|\psi\rangle_\alpha} = W(\beta - \alpha)_{|\psi\rangle}. \quad (4.1)$$

So the Q-function and the Wigner function of the state  $||\eta, M\rangle$  are easily obtained from those of the photon-added coherent states given in [5]

$$Q(\beta) = |\langle\beta||\eta, M\rangle|^2 = \frac{e^{-|\beta|^2} |\lambda + \beta|^{2M}}{M! L_M(-\lambda^2)}, \quad (4.2)$$

$$W(\beta) = \frac{2(-1)^M L_M(|2\beta + \lambda|^2)}{\pi L_M(-\lambda^2)} \exp(-2|\beta|^2). \quad (4.3)$$

The Q-function Eq.(4.2) has a  $2M$ -fold zero at the position  $\beta = -\lambda$ , which signals the nonclassical behaviour<sup>1</sup>. These zeros are related to the negative parts of the Wigner function, since the Q-function can be defined as a smoothed Wigner function. Fig.4 gives plots of the Wigner function of  $||\eta, M\rangle$  for  $M = 3$  and different  $\eta$ . One can clearly see the negative parts, except for the case  $\eta = 0$  which corresponds to the vacuum state whose Wigner function is simply a Gaussian centered at the origin. As  $\eta$  increases from 0, the Gaussian distribution continuously deforms to the Wigner function of the number state  $|3\rangle$ .

We can also study squeezing properties from the Q-function by examining the deformation of its contours. Fig.5 is the contour plot of Q functions for  $M = 10$  and different  $\eta$ . We see that, when we increase  $\eta$ , the contour is squeezed in the  $x$  direction until a maximum squeezing is reached. Then the contour deforms to the shape of a banana, which occupies a wider range in the  $x$  direction and the squeezing is reduced. Finally, we obtain a circular contour for larger  $\eta$  corresponding to no squeezing (c.f. Fig.2).

---

<sup>1</sup>We thank the referee for this remark.

## 5 Generation of intermediate states

The main difference between the intermediate states described herein and photon-added coherent states is that the former are a *finite* superposition of number states. This suggests the possibility of an experiment to produce these states using the method proposed in [11].

We can also generate the state  $||\eta, M\rangle$  by using the interaction of a photon and a two-level atom with an external classical driving field  $A$  in a cavity. In the rotating wave approximation, the Hamiltonian( $\hbar = 1$ ) is

$$\begin{aligned} H &= H_0 + V, \\ H_0 &= \omega N + A(a^\dagger + a) + \frac{1}{2}\omega_0\sigma_3, \\ V &= g(a^\dagger\sigma_- + a\sigma_+), \end{aligned} \quad (5.1)$$

where  $\sigma_3 = |e\rangle\langle e| - |g\rangle\langle g|$ ,  $\sigma_+ = |e\rangle\langle g|$  and  $\sigma_- = |g\rangle\langle e|$  are atomic operators,  $g$  is the one-photon coupling constant,  $\omega_0$  and  $\omega$  are the atomic transition frequency and cavity resonant mode frequency respectively, and we take the driving field  $A$  to be real and constant. The interaction Hamiltonian is

$$H_I(t) = U_0^{-1}(t)VU_0(t), \quad U_0(t) = e^{-iH_0t} = e^{-i/2\omega t N - iAt(a^\dagger + a)} e^{-i\omega_0 t \sigma_3}. \quad (5.2)$$

Using the following relation (see Appendix B)

$$U_0^{-1}(t)aU_0(t) = e^{-i\omega t} D(-A/\omega)aD(A/\omega), \quad (5.3)$$

where  $D(A/\omega)$  is the displacement operator, we have

$$H_I(t) = gD(-A/\omega) \left( e^{i(\omega-\omega_0)t} a^\dagger \sigma_- + e^{-i(\omega-\omega_0)t} a \sigma_+ \right) D(A/\omega). \quad (5.4)$$

Now we consider the on-resonance case,  $\omega = \omega_0$ . Then the interaction Hamiltonian is time-independent

$$H_I = gD(-A/\omega)(a^\dagger\sigma_- + a\sigma_+)D(A/\omega) \quad (5.5)$$

and therefore its time evolution operator is

$$U_I(t) = e^{-iH_I t} = D(-A/\omega)e^{-igt(a^\dagger\sigma_- + a\sigma_+)}D(A/\omega). \quad (5.6)$$

Suppose that the field is initially prepared in the vacuum state  $|0\rangle$  and the atom in the excited state  $|e\rangle$ ; namely, at  $t = 0$ , the system is in the state  $|0\rangle \otimes |e\rangle$ . At time  $t$  we have

$$U_I(t)|0\rangle \otimes |e\rangle = D(-A/\omega)e^{-igt(a^\dagger\sigma_- + a\sigma_+)}D(A/\omega)|0\rangle \otimes |e\rangle. \quad (5.7)$$

When  $gt \ll 1$ , we have

$$U_I(t)|0\rangle \otimes |e\rangle = |0\rangle \otimes |e\rangle - igt \left[ D(-A/\omega)a^\dagger D(A/\omega)|0\rangle \right] \otimes |g\rangle. \quad (5.8)$$

If the atom is detected in the ground state  $|g\rangle$ , the field is reduced to the state  $||\eta, 1\rangle$  with  $\eta = \omega^2/(A^2 + \omega^2)$ .

The state  $||\eta, M\rangle$  ( $M > 1$ ) can be generated by a multiphoton generalization of the Hamiltonian Eq.(5.1), namely,  $V = g(a^{\dagger M}\sigma_- + a^M\sigma_+)$ .

Note that the parameter  $A$  depends on the external driving field and is a tunable parameter. In particular, for large enough  $M$ , we can control the output state to be either a number or a coherent state by tuning the parameter  $A$ .

Finally we may infer the presence of these new intermediate states to first order in an idealized non-linear optics experiment. Consider a nonlinear Mach-Zehnder interferometer with a Kerr medium in one arm. The output state is the displaced Kerr state [12]

$$D(\xi)U_K(\gamma)|\lambda\rangle, \quad U_K(\gamma) \equiv \exp\left(\frac{i}{2}\gamma a^{\dagger 2}a^2\right), \quad (5.9)$$

where  $D(\xi)$  is the displacement operator and  $\gamma \equiv 2\chi L/v$ ,  $L$  is the length of the Kerr medium,  $v$  the appropriate phase velocity inside the medium and  $\chi$  the third-order susceptibility. When  $\xi = -\lambda$ , and  $\gamma$  is small enough, the above states can be approximated as

$$|0\rangle + \frac{i}{2}\gamma\lambda^2||\lambda, 2\rangle \quad (5.10)$$

showing the presence of the state  $|\eta, 2\rangle$  in first order. In general, if we use a  $(2S+1)$ th-order nonlinear Kerr medium modelled in the interaction picture by [13]

$$H_{\text{Kerr}} = \frac{\hbar\gamma_S}{(S+1)!}(a^\dagger)^{S+1}a^{(S+1)} = \frac{\hbar\gamma_S}{(S+1)!}N(N-1)\dots(N-S), \quad (5.11)$$

we can find  $||\eta, M\rangle$  when  $\gamma_S$  is small enough.

## 6 Interaction with a two-level atomic system

In this section we turn to the interaction of the state  $||\eta, M\rangle$  with a simple two-level system in the framework of the two-photon Jaynes-Cummings model (JCM) [14, 15] described by the following Hamiltonian ( $\hbar = 1$ )

$$H = \omega a^\dagger a + \frac{1}{2}\omega_0\sigma_3 + g(a^{\dagger 2}\sigma_- + a^2\sigma_+) = H_0 + V \quad (6.1)$$

with

$$H_0 = \omega a^\dagger a + \frac{1}{2}\omega_0\sigma_3, \quad V = g(a^{\dagger 2}\sigma_- + a^2\sigma_+).$$

The notation is as in Eq.(5.1), but now  $g$  is the two-photon coupling constant for transition  $|g\rangle \rightleftharpoons |e\rangle$ . Suppose that, at the initial time  $t = 0$ , atom and field are decoupled and the atom is initially in the excited state  $|e\rangle$ , while the field is in the intermediate number-coherent state  $||\eta, M\rangle$ . Then the combined atom-field wave function at time  $t$  is obtained as

$$|\psi_I(t)\rangle = \sum_{n=0}^M C_n(\eta, M) [\cos(\delta_n t) - i \frac{\Delta}{2\delta} \sin(\delta_n t)] e^{i\frac{\Delta}{2}t} |e\rangle \otimes |n\rangle - i \sum_{n=0}^M \frac{\Omega_n}{\delta_n} C_n(\eta, M) \sin(\delta_n t) e^{-i\frac{\Delta}{2}t} |g\rangle \otimes |n+2\rangle, \quad (6.2)$$

where

$$\Omega_n = g\sqrt{(n+1)(n+2)}, \quad \delta_n = \sqrt{\frac{\Delta^2}{4} + \Omega_n^2}, \quad \Delta = \omega_0 - 2\omega. \quad (6.3)$$

For simplicity, we only consider the on-resonance interaction case  $\Delta = 0$  as in [18] whereupon Eq.(6.2) simplifies to

$$|\psi_I(t)\rangle = \sum_{n=0}^M C_n(\eta, M) \cos(\Omega_n t) |e\rangle \otimes |n\rangle - i \sum_{n=0}^M C_n(\eta, M) \sin(\Omega_n t) |g\rangle \otimes |n+2\rangle. \quad (6.4)$$

We now discuss some quantum characteristics of the system arising from the equation Eq.(6.4).

## 6.1 Atomic population inversion

Atomic population inversion is an important atomic observable in the JCM and is defined as the difference between the probabilities of finding the atom in the excited state and in the ground state. From Eq.(6.4), the atomic population inversion is obtained as

$$W(t) = \langle \sigma_3 \rangle = \sum_{n=0}^M |C_n(\eta, M)|^2 \cos(2\Omega_n t). \quad (6.5)$$

Fig. 6 gives the inversion vs. scaled time  $\tau \equiv gt$  for different  $M$  and  $\eta$ . From Fig. 6, we observe that the atomic population inversion exhibits the conventional Rabi oscillation for the  $M$ -number state limit ( $\eta \rightarrow 1$ ). In fact, in the limit  $\eta \rightarrow 1$ , Eq. (6.5) is simplified as

$$W(t) = \cos(2\Omega_M t) \quad (6.6)$$

with frequency  $2\Omega_M = 2g[(M+1)(M+2)]^{1/2} (\approx 2Mg$  for high enough  $\langle N \rangle$ , see Fig.6(a)). In the coherent state limit we observe the collapse-revival phenomenon, as we expect, with a revival time  $t_{cs}$  which can be estimated as  $\pi/g$  [18] for high enough  $\langle N \rangle$  (that is, *revival frequency*  $\Omega_{cs} \equiv 2\pi/t_{cs} \approx 2g$ ) (Fig.6(d)). For the general intermediate case

(Fig.6(b,c)), remnants of both behaviour are seen; namely, an oscillation of frequency  $\Omega_M$  modulated by the frequency  $\Omega_{cs}$  with modulated amplitude dependent on the parameter  $\eta$  and  $M$ .

## 6.2 Field entropy

We now consider the cavity field observables, beginning with entropy which is a measure of the *amount of chaos* or lack of information about a system [16]. The entropy  $S$  of a quantum-mechanical system is defined as [17, 18]

$$S = -\text{Tr}(\rho \ln(\rho)),$$

where  $\rho$  is the density operator of the quantum system and the Boltzmann constant  $k$  is equal to unity. For a pure state,  $S = 0$ ; otherwise  $S > 0$ , and it increases with increasing number of microstates with decreasing statistical weight.

In this subsection we study the time evolution of the field entropy in our system. Barnett and Phoenix [17] have proved that the field entropy  $S_f$  equals the atomic entropy  $S_a$  if the total initial state is a pure state. From Eq.(6.4) the atomic reduced density operator  $\rho_a$  can be easily obtained as

$$\rho_a \equiv \text{Tr}_f(\rho) = \rho_{11}|g\rangle\langle g| + \rho_{12}|g\rangle\langle e| + \rho_{21}|e\rangle\langle g| + \rho_{22}|e\rangle\langle e|, \quad (6.7)$$

where

$$\begin{aligned} \rho_{11} &= \sum_{n=0}^M |C_n(\eta, M)|^2 \sin^2(\Omega_n t) \\ \rho_{22} &= \sum_{n=0}^M |C_n(\eta, M)|^2 \cos^2(\Omega_n t) \\ \rho_{12} = \rho_{21}^* &= \sum_{n=0}^{M-2} C_{n+2}(\eta, M) C_n(\eta, M) \cos(\Omega_{n+2} t) \sin(\Omega_n t). \end{aligned} \quad (6.8)$$

Then the field and atomic entropy  $S_a = -\text{Tr}_a(\rho_a \ln(\rho_a))$  can be expressed as

$$S_f = S_a = -\pi_+ \ln(\pi_+) - \pi_- \ln(\pi_-), \quad (6.9)$$

where  $\pi_{\pm}$  are eigenvalues of the atomic reduced field density operator  $\rho_a$

$$\pi_{\pm} = \frac{1}{2} (1 \pm \sqrt{(\rho_{22} - \rho_{11})^2 + 4|\rho_{12}|^2}). \quad (6.10)$$

The field entropy  $S_f$  as a function of  $\tau$  is presented in Fig.7. It is clear that  $S_f$  is a periodic function of time and it exhibits the conventional oscillation for the  $M$ -number state limit. As in the case of coherent initial states, the field entropy during

the time evolution is dynamically reduced to zero at revival time  $t_R$  which means the cavity field can be periodically found in pure states, and reaches a maximum at  $t_R/2$  and falls quickly to a minimum at  $\tau = \pi/4, 3\pi/4$ . Furthermore, for the general intermediate case, the field entropy has more minima as shown in Fig. 7 (b, c) due to the frequency modulation.

### 6.3 Q-function

The quasi-probability distribution Q-function is defined as [19]:

$$Q(\beta) = \frac{1}{\pi} \langle \beta | \rho_f | \beta \rangle,$$

where  $\rho_f = \text{Tr}_a(\rho)$  is the field reduced density operator

$$\begin{aligned} \rho_f = & \sum_{m,n=0}^M C_m(\eta, M) C_n(\eta, M) [\cos(\Omega_m t) \cos(\Omega_n t) |n\rangle \langle m| \\ & + \sin(\Omega_m t) \sin(\Omega_n t) |n+2\rangle \langle m+2|], \end{aligned} \quad (6.11)$$

and  $|\beta\rangle$  is the coherent state. So the Q-function of the cavity field is

$$Q(\beta) = \frac{e^{-|\beta|^2}}{\pi} \left( \left| \sum_{n=0}^M \frac{\beta^{*n}}{\sqrt{n!}} C_n(\eta, M) \cos(\Omega_n t) \right|^2 + \left| \sum_{n=0}^M \frac{(\beta^*)^{n+2}}{\sqrt{(n+2)!}} C_n(\eta, M) \sin(\Omega_n t) \right|^2 \right). \quad (6.12)$$

In Fig. 8 we give contour plots of the Q-function at different times  $\tau$  for  $\eta = 0.1, 0.8$ . At time  $\tau = 0$ , the Q-function has only a single peak and the field is in the pure quantum state  $|\eta, M\rangle$  (c.f. Fig. 5). With the development of time, the Q-function begins to separate into two peaks. The smaller  $\eta$ , the faster the separation. At time  $\tau = \pi/2$ , the Q-function exhibits the most separation and the field is in a mixed state since the entropy reaches its maximum. Then two peaks begins to merge together and finally combine in a single peak at time  $\tau = \pi$ , where the field is in a pure state with vanishing entropy.

### 6.4 Photon number distribution

The photon number distribution  $P_n(t)$  of the field described by the reduced density matrix  $\rho_f$  is given by

$$P_n(t) = \langle n | \rho_f | n \rangle. \quad (6.13)$$

Inserting Eq.(6.11) into Eq.(6.13) we find the photon number distribution at time  $t$

$$P_n(t) = |C_n(\eta, M)|^2 \cos^2(\Omega_n t) + |C_{n-2}(\eta, M)|^2 \sin^2(\Omega_{n-2} t). \quad (6.14)$$

Fig. 9 shows the behaviour of the photon number distribution at times  $\tau = 0, \pi/4, \pi/2, 3\pi/4$  and  $\pi$ . From these figures we can observe that the photon number distribution exhibits strong oscillation at time  $\tau = \pi/4$  and  $3/4\pi$  for the intermediate states. In fact, at those times, the field is a superposition of two components (see Fig.8) and its entropy decreases rapidly to a minimum (see Fig.7). Partial interference between two component results in strong oscillation of the photon number distribution. However, the oscillation is not *perfect* (see below). Nevertheless it is perfect at the slightly earlier time  $\tau = \pi/4 - \xi$  (see dashed lines in Fig.9(a,b)).

This effect is not hard to understand. In fact, at  $\tau = \pi/4$ , we have the following approximate result (see Appendix C)

$$P_n(t) = \left[ 1 + \frac{(1 - \eta)^2 n(n - 1)}{\eta^2 (M - n + 2)^2 (M - n + 1)^2} \right] |C_n(\eta, M)|^2 \sin^2 \left[ \left( n - \frac{1}{2} \right) \tau \right]_{\tau = \frac{\pi}{4}} \quad (6.15)$$

for the high enough  $\langle N \rangle$  case. Eq.(6.15) is a strongly oscillating function which explains the large oscillations of the photon number distribution. However, due to the additional term  $\tau/2 = \pi/8$ , the function  $\sin^2[(n - 1/2)\tau]_{\tau = \pi/4}$  cannot be zero for any integer  $n$ ; in other words, the oscillation is not perfect. However,  $P_n(t)$  is zero at the slightly earlier time  $\tau = \pi/4 - \xi$ , where  $\xi$  is chosen to make  $(n - 1/2)\tau$  a multiple of  $\pi$ .

From Fig.9(c) we also observe that the photon number distribution at  $\tau = \pi$  is simply a displacement by 2 from that at the time  $\tau = 0$ . For the large photon number case, this fact can be proved analytically. Using Eq. (C.4) in Appendix C, we have

$$\begin{aligned} \sin(\Omega_{n-2}t) &\approx \sin(n\pi - \pi/2) = (-1)^{n+1}, \\ \cos(\Omega_n t) &\approx \cos[(n + 1)\pi + \pi/2] = 0. \end{aligned}$$

So the photon number distribution Eq.(6.14) at  $\tau = \pi$  becomes

$$P_n(\pi/g) = |C_{n-2}(\eta, M)|^2 \equiv P_{n-2}(0). \quad (6.16)$$

In the same way we find that, at  $\tau = \pi/2$ , the photon number distribution is

$$P_n(\pi/2g) = \frac{1}{2} \left( |C_n(\eta, M)|^2 + |C_{n-2}(\eta, M)|^2 \right) = \frac{1}{2} (P_n(0) + P_n(\pi/g)), \quad (6.17)$$

namely, the *average* of the photon number distributions at  $\tau = 0$  and  $\tau = \pi$ . In Fig.9(c) this fact can be clearly observed.

## 7 Conclusion

In this paper we have described new states  $|\eta, M\rangle$  which interpolate between number and coherent states and have investigated their various properties. Unlike photon-added

coherent states, to which they are related, these states are a *finite* superposition of number states. We also analyzed the limiting cases  $\eta \rightarrow 1$  and  $\eta \rightarrow 0$ ,  $M \rightarrow \infty$  corresponding to number and coherent states respectively. Salient statistical properties of  $||\eta, M\rangle$  such as the sub-Poissonian distribution, the anti-bunching effect and the squeezing effects were investigated for a wide range of parameters. The non-classical features of these states for certain parameter ranges were demonstrated in terms of the quasiprobability distributions, the Q and Wigner functions. We also proposed an experiment to generate these states, inferring their presence in certain non-linear systems.

We then considered the interaction of these interpolating number-coherent states with a two-level atomic system, exemplified by the two-photon Jaynes-Cummings Model. We first studied the dynamics of atomic population inversion. On an intuitive level, one expects that the response of the atomic system will vary between the Rabi oscillation typical of an initial number state, and the collapse-revival mode for an initial coherent state; and indeed this is what one obtains. We found that it exhibited the conventional Rabi oscillation for the  $M$ -number state limit with frequency  $\Omega_M$  ( $\approx 2Mg$ ) and the collapse-revival phenomenon for the coherent state limit with revival frequency  $\Omega_{cs} \approx 2g$ . For the general intermediate case, remnants of both behavior were seen; namely, an oscillation of frequency  $\Omega_M$  modulated by the frequency  $\Omega_{cs}$  with modulated amplitude dependent on the parameter  $\eta$  and  $M$ .

We further investigated the field observables, the entropy, Q-function and photon number distribution. It is of interest that the photon number distribution exhibit strong oscillation at  $\tau = \pi/4, 3\pi/4$ . At those times, the field entropy falls rapidly to a minimum and the Q-function separates into two peaks, which means that the field is a superposition of almost pure states and interference between components of the superposition state leads to strong oscillation of the photon number distribution. An approximate analytical solution is presented to explain this result.

The remarkable properties of these intermediate number-coherent states provide a useful tool for theoretical investigation of model systems; their generation by non-linear systems tempts us to believe that the states found in this paper may play an important role in quantum optics.

## Acknowledgements

H. Fu is supported in part by the National Natural Science Foundation of China. We would like to thank Dr.A.Greentree of the Quantum Processes Group of the Open Uni-

versity for enlightening discussion on the production of these states, and the referee for valuable comments.

## References

- [1] Stoler D, Saleh B E A and Teich M C 1985 *Opt. Acta* **32** 345
- [2] C. T. Lee, *Phys. Rev.* **31A**, (1985) 1213.  
A. V. Barranco and J. Roversi, *Phys. Rev.* **50A** (1994) 5233;  
B. Baseia, A. F. de Lima and A. J. da Silva, *Mod. Phys. Lett. B* **9** (1995) 1673;  
B. Baseia, A. F. de Lima and G. C. Marques, *Phys. Lett. A* **204** (1995) 1;  
H. Y. Fan and S. J. Jing, *Phys. Rev. A.* **50** (1994) 1909;  
H. C. Fu, *J. Phys. A.*, **30**(1997)L83 and references therein.
- [3] H. C. Fu and R. Sasaki, *J. Phys. A.* **29** (1996) 5637.
- [4] T. Holstein and H. Primakoff, *Phys. Rev.* **58** (1940) 1048.  
J. Katriel, M. Rasetti and A. I. Solomon, *Phys. Rev. D.* **35** (1987) 2601.
- [5] G. S. Agarwal and K. Tara, *Phys. Rev. A* **43** (1990) 492.
- [6] I.S.Gradshteyn and I.M.Ryzhik, *Table of Integrals, Series and Products* (Academic, New York, 1965).
- [7] L. Mandel, *Opt. Lett.* **4** (1979) 205.
- [8] See for example, D. F. Walls and G. C. Millburn, *Quantum Optics* (Springer 1994).
- [9] H. P. Yuen, *Phys. Lett. A.* **56** (1976) 105.  
A. I. Solomon, *Phys. Lett. A.* **188** (1994) 215.  
Y. Feng and A. I. Solomon, *Opt. Commun.* **152** (1998) 299.
- [10] M. Hillery, R. F. O'Connell, M. O. Scully and E. P. Wigner, *Phys. Rep.* **106** (1984) 121.
- [11] J. Janszky, P. Domokos, S. Szabo and Adam *Phys. Rev.* **51A** (1995) 4191.
- [12] A. D. Wilson-Gordon, V. Bužek and P. L. Knight, *Phys. Rev. A* **44** (1991) 7647.
- [13] C. C. Gerry, *Phys. Lett. A* **124** (1987) 237; V. Bužek and I. Jex, *Acta Phys. Slov* **39** (1989) 351; M. Paprzycka and R. Tanaś, *Quantum Opt.* **4** (1992) 331.

- [14] Jaynes E.T. and Cummings F.W.(1963), *Proc. IEEE*, **51**, 89
- [15] Shore B.W. and Knight P.L.(1993), *J. Mod. Opt.* **40**, 1195
- [16] Alfred Wehrl(1978), *Rev. Mod. Phys.* **50**, 221
- [17] Barnett S.M.and Phoenix S.J.D.(1989), *Phys. Rev. A* **40**, 2042
- [18] Bužek V. and Hladký B.(1993), *J. Mod. Opt.* **40**, 1309
- [19] Glauber R.J.(1963), *Phys. Rev.* **130** , 2529 and **131**, 2766
- [20] H. Moya-Cessa and P. L. Knight, *Phys. Rev. A.* **28** (1993) 2479.

## Appendix A: Displaced quasiprobability distributions

For the Q-function, we prove Eq. (4.1) as follows:

$$\begin{aligned} Q(\beta)_{|\psi\rangle_\alpha} &= |\langle\beta|D(\alpha)|\psi\rangle|^2 = |\langle 0|D(-\beta)D(\alpha)|\psi\rangle|^2 \\ &= |\langle\beta - \alpha|\psi\rangle|^2 = Q(\beta - \alpha)_{|\psi\rangle}, \end{aligned} \quad (\text{A.1})$$

where we have used the relation

$$D(\delta)D(\gamma) = D(\delta + \gamma)e^{\frac{1}{2}(\delta\gamma^* - \gamma\delta^*)} = D(\delta + \gamma)e^{i\text{Im}(\delta\gamma^*)}, \quad (\text{A.2})$$

for arbitrary complex numbers  $\delta$  and  $\gamma$ . From the following definition of the Wigner function [20]

$$W(\beta) = \frac{2}{\pi} \sum_{k=0}^{\infty} \langle\beta, k|\rho|\beta, k\rangle, \quad (\text{A.3})$$

where  $|\beta, k\rangle \equiv D(\beta)|k\rangle = e^{\beta a^\dagger - \beta^* a}|k\rangle$  is the displaced number state ( $|k\rangle$  is the number state) and  $\rho = |\eta, M\rangle\langle\eta, M|$  is the density matrix of the states considered, we can prove the second relation in Eq.(4.1) in the same way as in the Q-function case.

## Appendix B: Proof of formula Eq.(5.3)

In this appendix we give a proof of Eq.(5.3). We use the following formula

$$e^{-F} G e^F = \sum_{n=0}^{\infty} \frac{(-1)^n}{n!} \underbrace{[F, [F, \dots, [F, G] \dots]]}_{n \text{ copies}}. \quad (\text{B.1})$$

For the case in hand

$$F = -i\omega t N - itA(a^\dagger + a), \quad G = a. \quad (\text{B.2})$$

It is easy to see that

$$\begin{aligned}
[F, G] &= i\omega ta + iAt, \\
[F, [F, G]] &= i\omega t[F, G], \\
[F, [F, [F, G]]] &= i\omega t[F, [F, G]] = (i\omega t)^2[F, G], \\
&\dots\dots \\
\underbrace{[F, [F, \dots, [F, G] \dots]]}_{n \text{ copies}} &= (i\omega t)^n[F, G] \\
&= (i\omega t)^n a + (i\omega t)^n A/\omega = (i\omega t)^n D(-A/\omega) a D(A/\omega), \tag{B.3}
\end{aligned}$$

where  $D(A/\omega)$  is the displaced operator. Substituting Eq. (B.3) into Eq. (B.1) we obtain the formula Eq.(5.3).

## Appendix C: Photon number distribution for large photon number

In this appendix we present an analytical treatment of the photon number distribution in the large photon number regime. The photon number distribution of the two-photon JC model with initial state  $|e\rangle \otimes \sum_n C_n |n\rangle$  can be obtained as

$$P_n(t) = |C_n|^2 \cos^2 \left( \sqrt{(n+1)(n+2)}\tau \right) + |C_{n-2}|^2 \sin^2 \left( \sqrt{(n-1)n}\tau \right), \tag{C.1}$$

where  $\tau = gt$  is the scaled time as before.

Here we only consider an initial field state which is narrower than that of a coherent state. For a distribution  $\{|C_n|^2\}$  we can calculate the variance as

$$(n - \bar{n})^2 = \langle N^2 \rangle - \langle N \rangle^2. \tag{C.2}$$

For the coherent state  $|\alpha\rangle$ , we have  $(n - \bar{n})^2 = \bar{n}$ . So for highly excited coherent states where  $\bar{n} \rightarrow \infty$ , we have  $n \sim \bar{n}$ . In the following we only consider a distribution  $\{|C_n|^2\}$  narrower than the Poisson distribution, namely

$$(n - \bar{n})^2 \leq \bar{n}. \tag{C.3}$$

So for large enough  $\bar{n}$  we also have  $n \sim \bar{n}$ . In this case, we have

$$\begin{aligned}
\sqrt{(n+1)(n+2)} &\approx \sqrt{n^2 + 3n} = n\sqrt{1 + \frac{3}{n}} = n + \frac{3}{2} = \left(n - \frac{1}{2}\right) + 2, \\
\sqrt{(n-1)n} &\approx \sqrt{n^2 - n} = n\sqrt{1 - \frac{1}{n}} = n - \frac{1}{2}. \tag{C.4}
\end{aligned}$$

Futhermore, when  $\tau = \pi/4$  we have

$$\cos^2 \left( \sqrt{(n+1)(n+2)\tau} \right) = \cos^2 \left[ \left( n - \frac{1}{2} \right) \tau + \frac{\pi}{2} \right]_{\tau=\frac{\pi}{4}} = \sin^2 \left[ \left( n - \frac{1}{2} \right) \tau \right]_{\tau=\frac{\pi}{4}}. \quad (\text{C.5})$$

Substituting Eq.(C.5) into Eq.(C.1) we obtain the approximate photon number distribution at  $\tau = \pi/4$

$$P_n(t) = (|C_n|^2 + |C_{n-2}|^2) \sin^2 \left[ \left( n - \frac{1}{2} \right) \tau \right]_{\tau=\frac{\pi}{4}}. \quad (\text{C.6})$$

From Eq.(C.6) we find that, for the initial field whose photon distribution is narrower than a Poisson distribution, the photon number distribution at  $\tau = \pi/4$  exhibits strong oscillation. However,  $P_n(\pi/4)$  cannot be zero for any  $n$  due to the term  $\tau/2 = \pi/8$  and the oscillation is not perfect. Nevertheless, the oscillation is perfect at a slightly earlier time  $\tau = \pi/4 - \xi$ , as indicated in Ref.[18] (for initial coherent state) and Fig.9(a,b).

For coherent states we further have  $|C_{n-2}|^2 \approx |C_n|^2$ . So the photon number distribution is

$$P_n(t) = 2e^{-\bar{n}} \frac{\bar{n}^n}{n!} \sin^2 \left[ \left( n - \frac{1}{2} \right) \tau \right]_{\tau=\frac{\pi}{4}}, \quad (\text{C.7})$$

which is just the result given in Ref. [18].

Now we turn to the analytical approximate result Eq.(6.15). For the intermediate state, we can write the variance as

$$(n - \bar{n}_M)^2 = \langle N \rangle_{M-1} \langle N \rangle_M - \langle N \rangle_M^2 + \langle N \rangle_M, \quad (\text{C.8})$$

where  $\bar{n}_M \equiv \langle N \rangle_M \equiv \langle \eta, M | N | \eta, M \rangle$ . In general, we have  $\langle N \rangle_{M-1} \leq \langle N \rangle_M \leq M$ . For large enough  $\bar{n}_M$ , or  $M$ , we have  $\langle N \rangle_{M-1} \approx \langle N \rangle_M$  and therefore  $(n - \bar{n}_M)^2 \sim \bar{n}_M$  which leads to  $n \sim \bar{n}_M$ . So the result Eq.(C.6) is valid for the intermediate state case. Furthermore, the distribution  $|C_n(\eta, M)|^2$  and  $|C_{n-2}(\eta, M)|^2$  are related by

$$|C_{n-2}(\eta, M)|^2 = \frac{(1-\eta)^2 n(n-1)}{\eta^2 (M-n+2)^2 (M-n+1)^2} |C_n(\eta, M)|^2. \quad (\text{C.9})$$

Sunstituting Eq.(C.9) into Eq.(C.6), we finally obtain Eq.(6.15).

Eq.(C.4) can also be used to explain the behaviour of the photon number distribution at  $\tau = \pi/2$  and  $\pi$  (see Eqs.(6.16,6.17) and Fig.9).

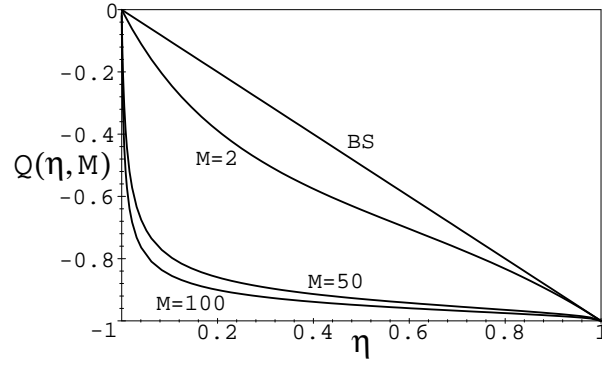


Figure 1: Mandel's  $Q$  parameter for  $M=2, 50, 100$ .

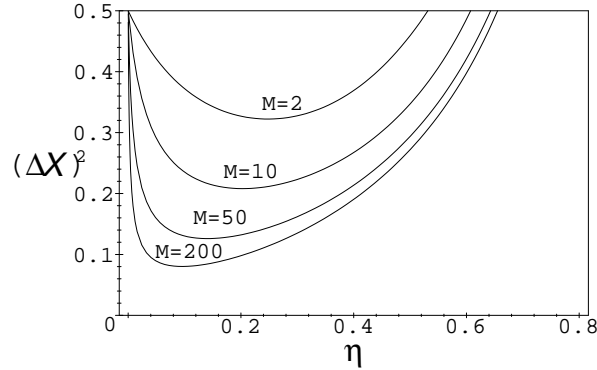


Figure 2: Variance  $(\Delta x)^2$  of  $||\eta, M\rangle$  as a function of  $\eta$  for  $M = 2, 20, 50,$  and  $200$ .

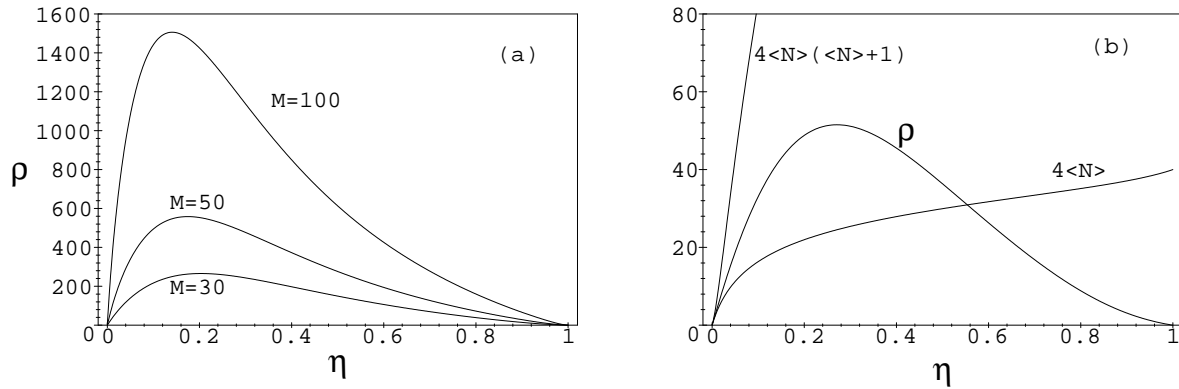


Figure 3: The signal-to-quantum noise ratio for  $||\eta, M\rangle$ : (a) The ratio for different  $M$ ; (b) Comparison of  $\rho$ ,  $4\langle N\rangle(\langle N\rangle + 1)$  and  $4\langle N\rangle$  for  $M = 10$ .

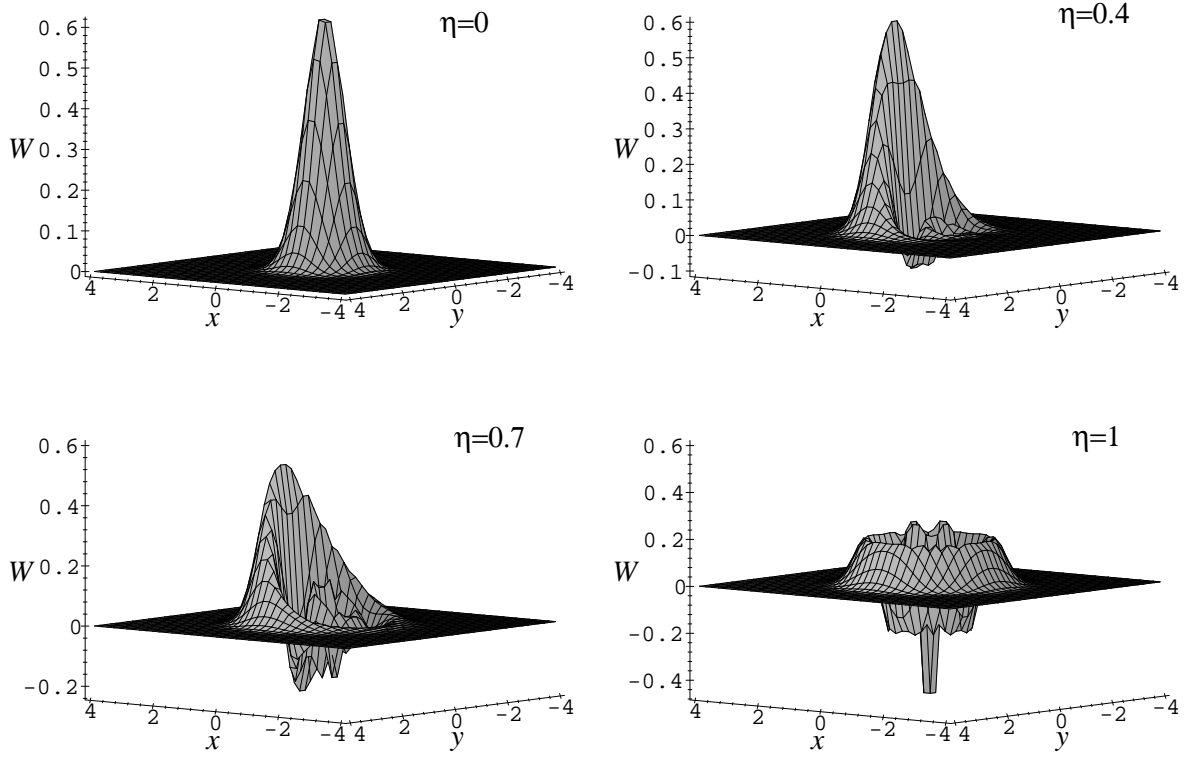


Figure 4: Wigner function of  $|\eta, M\rangle$  for  $M = 3$  and  $\eta = 0.1, 0.4, 0.7$  and  $1$ .  $\alpha = x + iy$ .

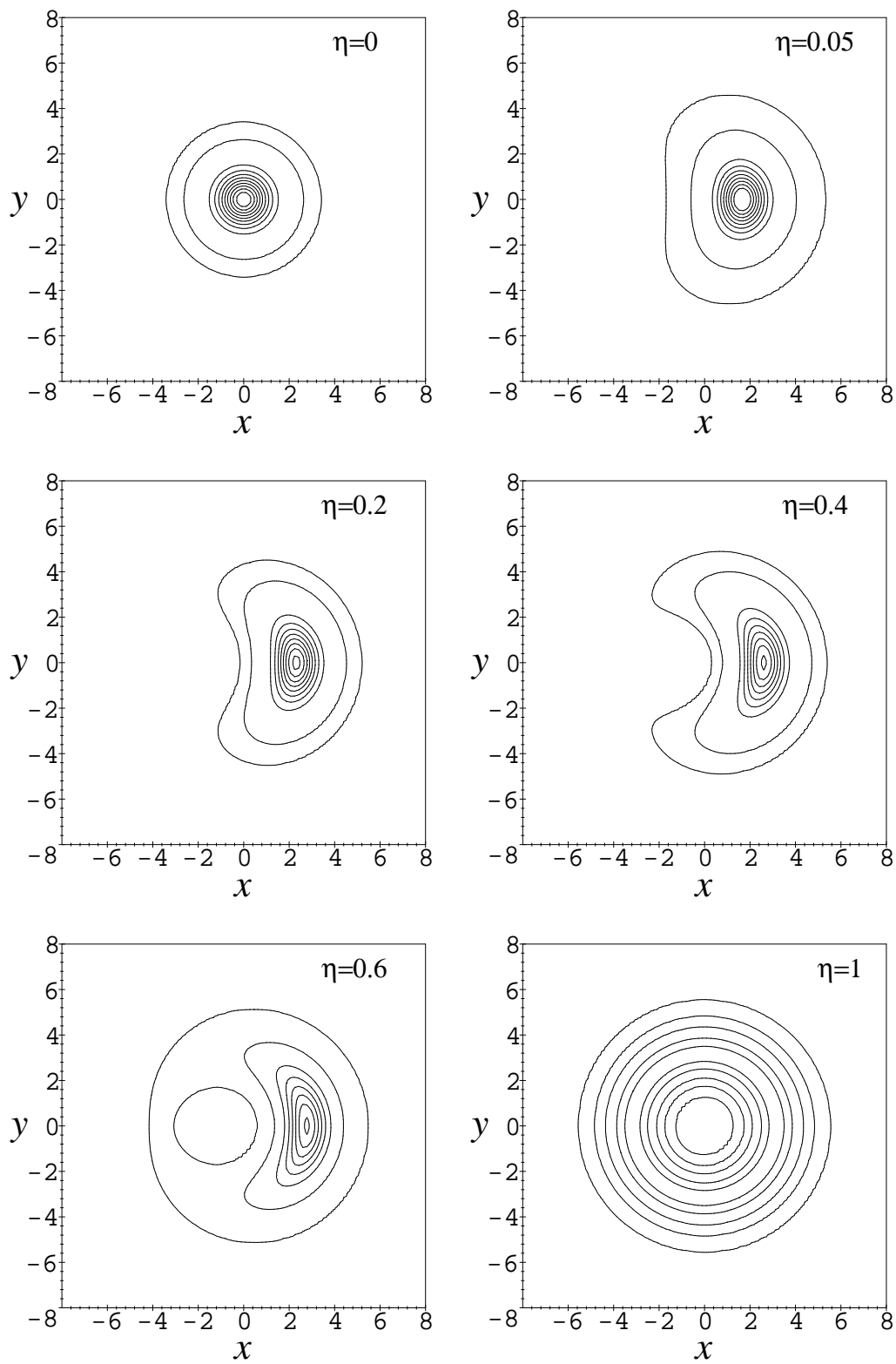


Figure 5: Contours of the Q-function of  $|\eta, M\rangle$ . In all cases  $M = 10$ .  $\alpha = x + iy$ .

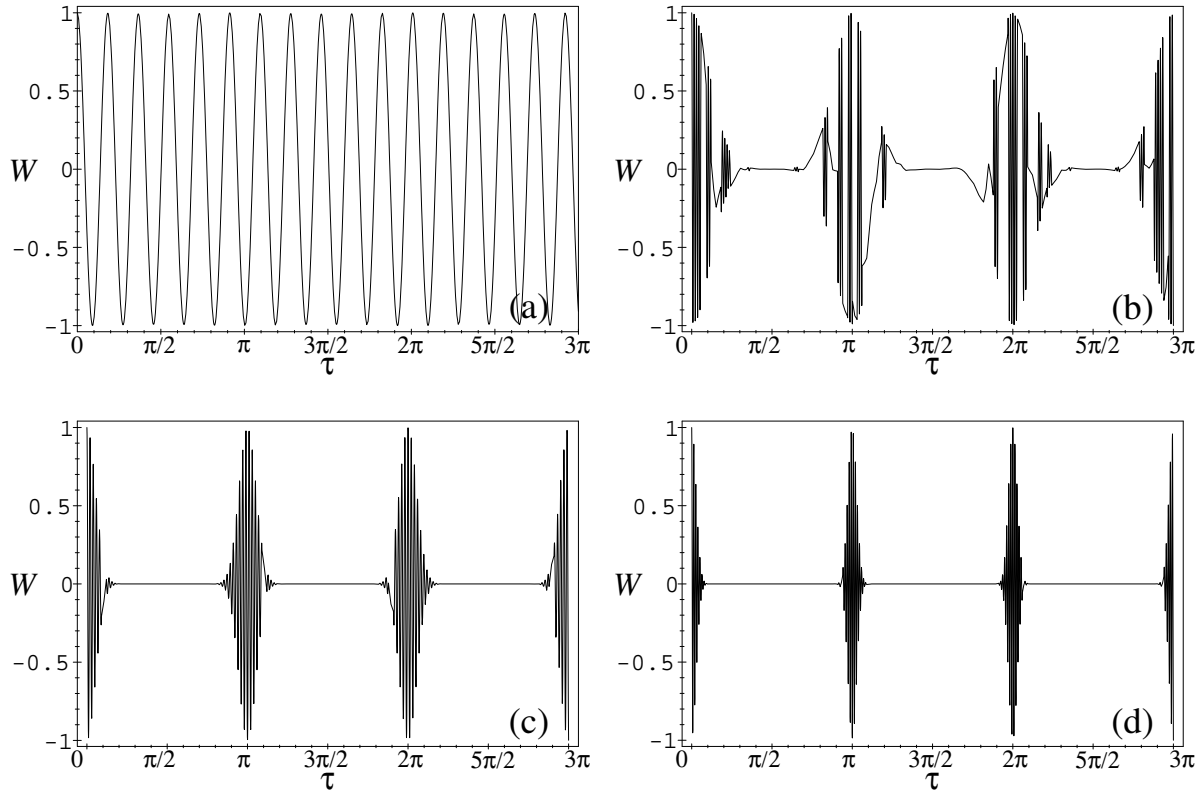


Figure 6: Atomic population inversion as a function of the scaled time  $\tau$ . (a)  $M = 4, \eta = 0.999$ ; (b)  $M = 70, \eta = 0.8$ ; (c)  $M = 70, \eta = 0.1$ ; (d)  $M = 200, \eta = 0.001$ .

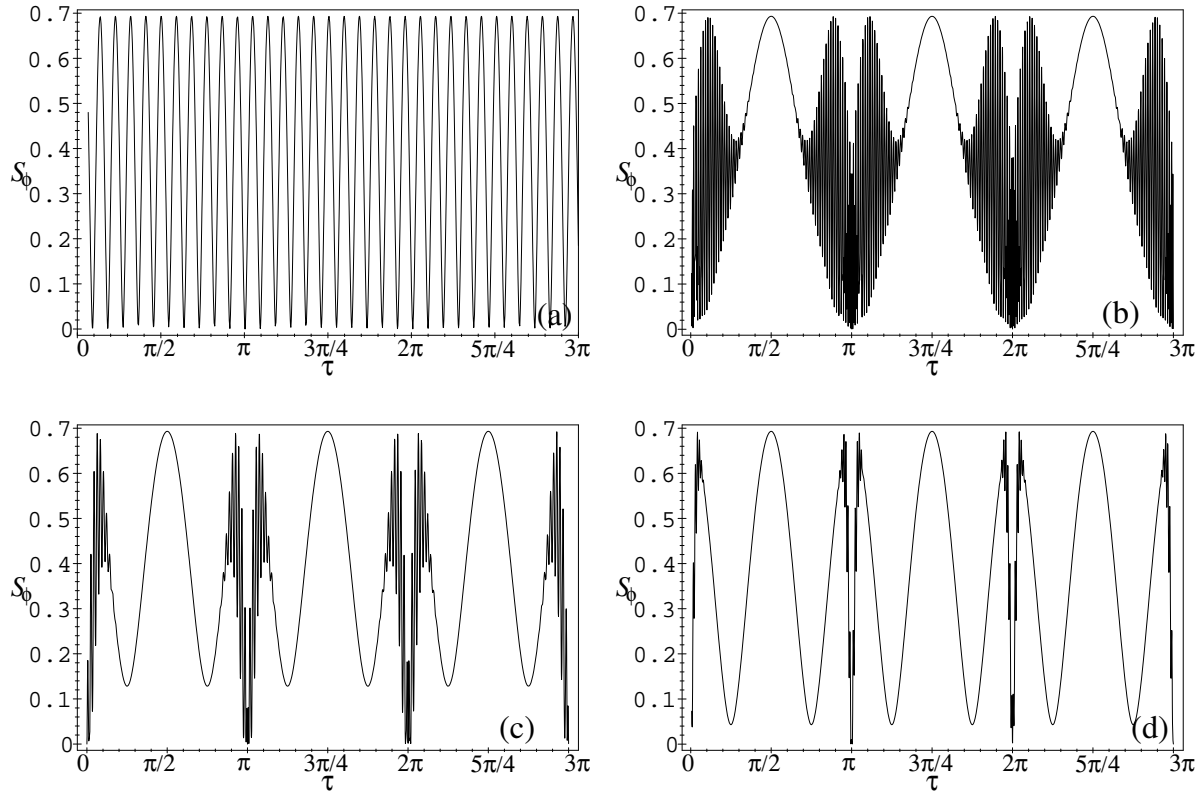


Figure 7: Entropy of the field as a function of scaled time  $\tau$ . (a)  $M = 4$  and  $\eta = 0.9999$  (the initial field state is the number state  $|4\rangle$ ); (b)  $M = 70$  and  $\eta = 0.8$ ; (c)  $M = 70$  and  $\eta = 0.1$ ; (d)  $M = 200$  and  $\eta = 0.005$ .

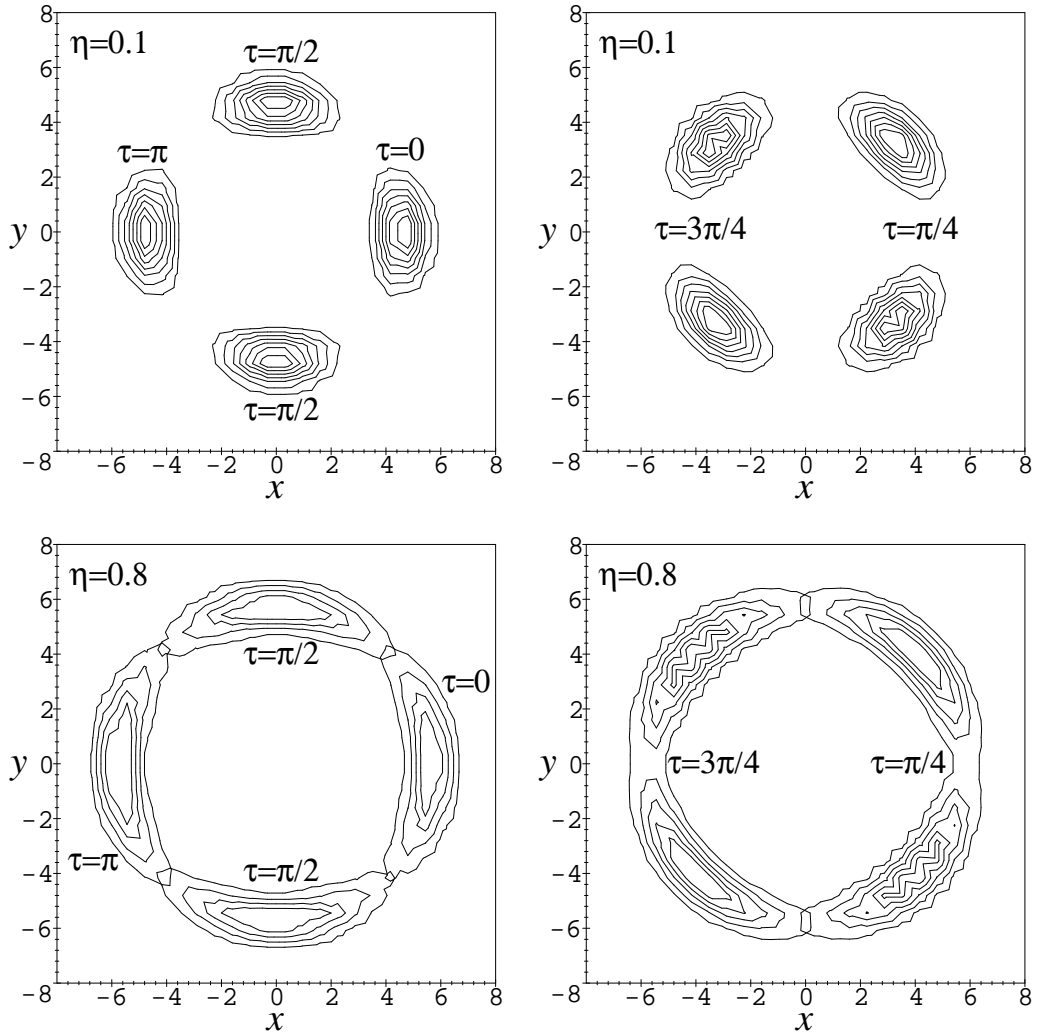


Figure 8: Contour plots of the Q-function of the field at  $\tau = 0, \pi/4, \pi/2, 3\pi/4$  and  $\pi$ . Here we choose  $\eta = 0.1, 0.8$ .

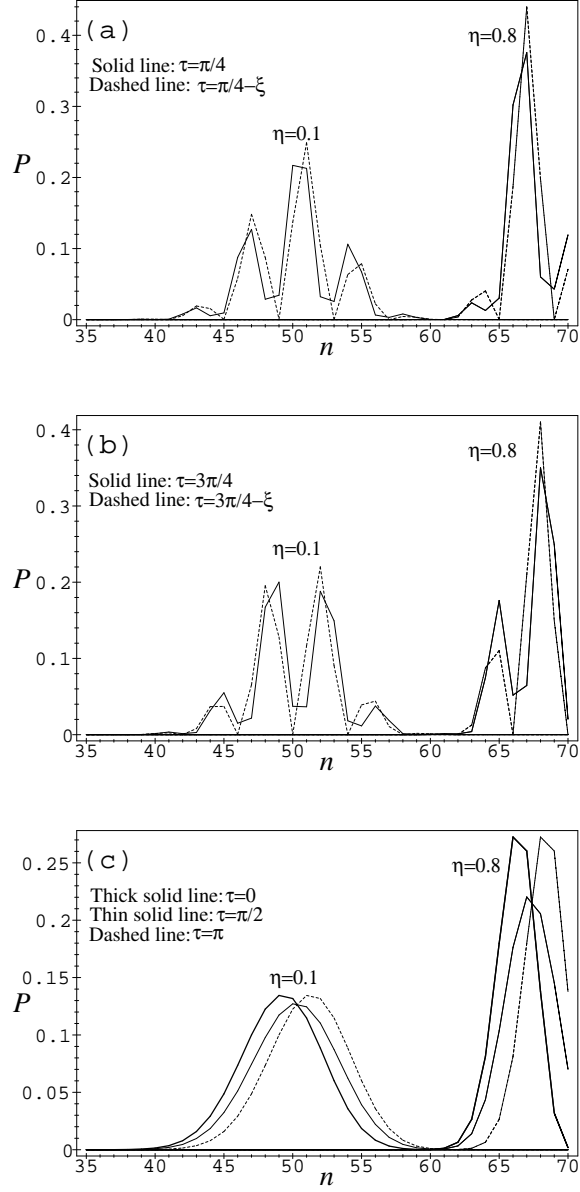


Figure 9: Number distribution of the photon field at different times  $\tau = 0, \pi/4, \pi/2, 3\pi/4$  and  $\pi$  for  $\eta = 0.1, 0.8$ . In (a) and (b) we also present the distribution at slightly earlier time  $\tau - \xi$ , where  $\xi$  is chosen as  $1/140$  and  $1/180$  for  $\eta = 0.1$  and  $\eta = 0.8$  respectively.